Geophysical Research Letters

RESEARCH LETTER
10.1029/2019GL082922

Observed El Niño-La Niña Asymmetry in a Linear Model

Cristian Martinez-Villalobos[1], Matthew Newman[2,3], Daniel J. Vimont[4], Cécile Penland[3], and J. David Neelin[1]

[1]Department of Atmospheric and Oceanic Sciences, UCLA, Los Angeles, CA, USA, [2]Cooperative Institute for Research in Environmental Sciences, University of Colorado Boulder, Boulder, Boulder, USA, [3]Physical Sciences Division, NOAA/Earth System Research Laboratory, Boulder, CO, USA, [4]Department of Atmospheric and Oceanic Sciences, University of Wisconsin-Madison, Madison, WI, USA

Key Points:
- El Niño-La Niña asymmetry, usually associated with deterministic nonlinearity, may also be generated by a stochastically forced linear model
- A linear model forced by "correlated additive-multiplicative noise" is empirically calculated from observed Tropical Pacific SST data
- Our linear model generates El Niño-La Niña amplitude and persistence asymmetry consistent with observations (5th–95th confidence interval)

Supporting Information:
- Supporting Information S1

Correspondence to:
C. Martinez-Villalobos,
cmartinezvil@atmos.ucla.edu

Citation:
Martinez-Villalobos C., Newman, M., Vimont, D. J., Penland, C., & Neelin, J. D. (2019). Observed El Niño-La Niña asymmetry in a linear model. *Geophysical Research Letters*, *46*, 9909–9919. https://doi.org/10.1029/2019GL082922

Received 20 MAR 2019
Accepted 19 JUL 2019
Accepted article online 29 JUL 2019
Published online 22 AUG 2019

Abstract Previous studies indicate an asymmetry in the amplitude and persistence of El Niño (EN) and La Niña (LN) events. We show that this observed EN-LN asymmetry can be captured with a linear model driven by correlated additive and multiplicative (CAM) noise, without resorting to a deterministic nonlinear model. The model is derived from 1-month lag statistics taken from monthly sea surface temperature (SST) data sets spanning the twentieth century, in an extension of an empirical-dynamical technique called Linear Inverse Modeling. Our results suggest that noise amplitudes tend to be stronger for EN compared to LN events, which is sufficient to generate asymmetry in amplitude and also produces more persistent LN events on average. These results establish a null hypothesis for EN-LN asymmetry and suggest that strong EN events may not be more predictable that what can be accounted for by a multivariate linear system driven by CAM noise.

1. Introduction

It is often noted that the El Niño Southern Oscillation (ENSO) phenomenon in the observed record is asymmetric between its positive (El Niño [EN]) and negative (La Niña [LN]) states. Extreme EN events tend to be more intense than extreme LN events (Burgers & Stephenson, 1999), and LN events tend to be more persistent (DiNezio & Deser, 2014; Hu et al., 2014; Ohba et al., 2010; Ohba & Watanabe, 2012; Okumura & Deser, 2010). ENSO asymmetry has been considered to represent nonlinearity within the Tropical Pacific system, with slow, deterministic nonlinear feedbacks between sea surface temperatures (SSTs), thermocline, and winds operating differently for EN than LN (e.g., An & Jin, 2004; DiNezio & Deser, 2014; Dong, 2005; Im et al., 2015; Jin et al., 2003; Kang & Kug, 2002; Liang et al., 2012; Meinen & McPhaden, 2000; Su et al., 2010). Implicit in this view is that the time scale of these nonlinear feedbacks is comparable to the typical SST decay time scale, and hence, a correct identification of the balance between these processes may lead to potential increases in predictability estimates, particularly of extremes.

Certainly, the primitive equations governing the evolution of the Tropical Pacific upper ocean conditions are nonlinear. Characterizing the nature of the nonlinear processes in terms of their dominant time scales, however, may yield improved understanding of the key contributors to ENSO variability and predictability. Nonlinear processes decorrelating with a time scale comparable to that of linear decay contribute to the deterministic part of the system. This includes the class of ENSO chaotic models (Chekroun et al., 2014; Jin et al., 1994; Tziperman et al., 1994). On the other hand, temporally coarse graining the primitive equations (focusing on monthly SST anomalies, e.g.) tends to average out the details of those nonlinear processes decorrelating rapidly relative to linear dynamics (Hasselmann, 1976; Penland, 1996). In this case, a stochastic *approximation* of these processes as white noise, which may include a multiplicative (state-dependent) component, is appropriate (Sardeshmukh & Penland, 2015; Sardeshmukh et al., 2003; Majda et al., 2008).

Several previous studies have demonstrated that multiplicative noise may be used to model fast atmospheric processes key to ENSO development (e.g., Blanke et al., 1997; Bianucci et al., 2018; Christensen et al., 2017; Kleeman & Moore, 1997; Jin et al., 2007), including surface flux dependence on rapid wind variability (Sardeshmukh & Penland, 2015; Sura et al., 2006; Sura & Newman, 2008; Williams, 2012), westerly wind bursts (WWBs; Levine & Jin, 2017; Thual et al., 2016), and variability associated with the convective envelope of the Madden Julian Oscillation (Kapur & Zhang, 2012; Perez et al., 2005). Also, these fast processes may act differently during EN and LN events (Capotondi et al., 2018; Kug et al., 2008); that is, the

noise is also asymmetric. For example, ocean-atmosphere surface fluxes tend to be enhanced for unstable conditions (e.g., Sura et al., 2006), which are more likely to occur over warm SST anomalies. Additionally, WWBs (which often occur in association with Madden Julian Oscillation events; see Puy et al., 2016) are known to occur more frequently during EN events, and their interaction with SST anomalies acts as a short time scale positive feedback increasing the probability of large positive ENSO events (Eisenman et al., 2005; Gebbie et al., 2007; Lengaigne et al., 2004; Lopez et al., 2013; Vecchi & Harrison, 2000), consequently skewing ENSO statistics (Jin et al., 2007; Levine et al., 2016).

For a system whose *deterministic* dynamics are effectively linear, state-dependent asymmetric noise can nevertheless drive non-Gaussian statistics (Sardeshmukh & Sura, 2009, hereafter SS09) and, importantly, a corresponding asymmetry in the duration of positively and negatively signed events (Sardeshmukh et al., 2015; hereafter SCP15). This leads us to ask whether observed EN-LN asymmetry (e.g., An & Jin, 2004; Burgers & Stephenson, 1999) can likewise be understood in the context of a linear dynamical system forced with linearly state-dependent white noise. Past analyses have used a Linear Inverse Model (LIM; Penland & Sardeshmukh, 1995, hereafter PS95), to empirically extract a linear dynamical system forced with state-*independent* (i.e., additive) white noise from the covariance statistics of Tropical Pacific anomalies. Such a LIM can still explain ENSO irregularity (PS95), the (nonnormal) cycle of ENSO decay and growth (PS95, Vimont et al., 2014), the spectral characteristics of the main ENSO indices (Ault et al., 2013; Newman et al., 2009) and has also been shown to have forecast skill comparable to that of fully coupled, nonlinear General Circulation Models (Newman & Sardeshmukh, 2017), suggesting that it provides a good approximation to the Tropical Pacific deterministic dynamics at time scales relevant for ENSO (PS95; see also Penland, 2010). Moreover, inverse models augmented with deterministic nonlinearity do not seem to improve forecast skill over their linear counterparts (Chen et al., 2016; Kondrashov et al., 2005), which suggests that nonlinear processes contribute mostly to the unpredictable part of the system. However, a LIM forced by additive white noise captures neither the observed state dependence of noise processes nor the observed EN-LN asymmetry in event amplitude and duration. This has been a significant limitation of past LIM studies of ENSO, due to a lack of estimation methods for determining noise state dependence in the multivariate case. In this paper we use the parameters estimation method described in Martinez-Villalobos et al., 2018 (2018; hereafter M18; see also Martinez-Villalobos, 2016) to formulate a LIM, constructed from centennial-length records of observed SST anomalies, that now includes correlated additive-multiplicative (CAM) noise (SS09), which is an empirical estimate of the net effect of all noise processes with asymmetric dependence upon ENSO states. This new tropical Pacific "CAM-LIM" is then used to show that observed EN-LN asymmetry in both amplitude and duration can be consistent with predictably linear dynamics.

2. LIM Driven by CAM Noise (CAM-LIM)

To model Tropical Pacific SST anomalies, we consider two variants of multivariate Markov models. The first one, which we refer to as the standard LIM (PS95), is given by

$$\frac{\mathrm{d}\mathbf{x}}{\mathrm{d}t} = \mathbf{M}\mathbf{x} + \mathbf{B}\eta, \tag{1}$$

where $\mathbf{x}$ is the state vector of Tropical Pacific SST anomalies, $\mathbf{M}$ is a constant and stable matrix encoding the deterministic dynamics, $\mathbf{B}$ is a constant noise amplitude matrix, and η is a vector of centered Gaussian white noise processes ($\langle \eta_j(t) \rangle = 0$, $\langle \eta_j(t)\eta_k(t') \rangle = \delta(t-t')\delta_{jk}$). This noise forcing parameterizes the unpredictable portion of short-lived chaotic and nonlinear processes influencing SST evolution. The second Markov model, referred to as the CAM-LIM (M18), is given by

$$\frac{\mathrm{d}\mathbf{x}}{\mathrm{d}t} = \mathbf{A}\mathbf{x} + \mathbf{B}^{\mathbf{A}}\eta^{\mathbf{A}} + \mathbf{B}^{\mathbf{M}}(\mathbf{x})\eta^{\mathbf{M}} - \mathbf{D}, \tag{2}$$

which is a multivariate version of the CAM-noise linear model first introduced by SS09 and further evaluated by SCP15. Here $\mathbf{A}$ is a constant and stable matrix, $\mathbf{B}^{\mathbf{A}}$ and $\mathbf{B}^{\mathbf{M}}$ are constant and linear state-dependent noise amplitude matrices, respectively, $\eta^{\mathbf{A}}$ and $\eta^{\mathbf{M}}$ are vectors of centered Gaussian white noise processes, and $-\mathbf{D}$ eliminates the mean noise induced drift (SS09), which is zero in the standard LIM case. The term $\mathbf{B}^{\mathbf{M}}(\mathbf{x})\eta^{\mathbf{M}}$ represents the state-dependent noise forcing, which includes an additive component correlated to the multiplicative component, and $\mathbf{B}^{\mathbf{A}}\eta^{\mathbf{A}}$ represents the remaining additive noise.

Long time series are necessary to estimate multiplicative noise from data (M18, section 4c; Sura & Barsugli, 2002). Therefore, we construct both LIMs using only SST since while several available SST reconstructions

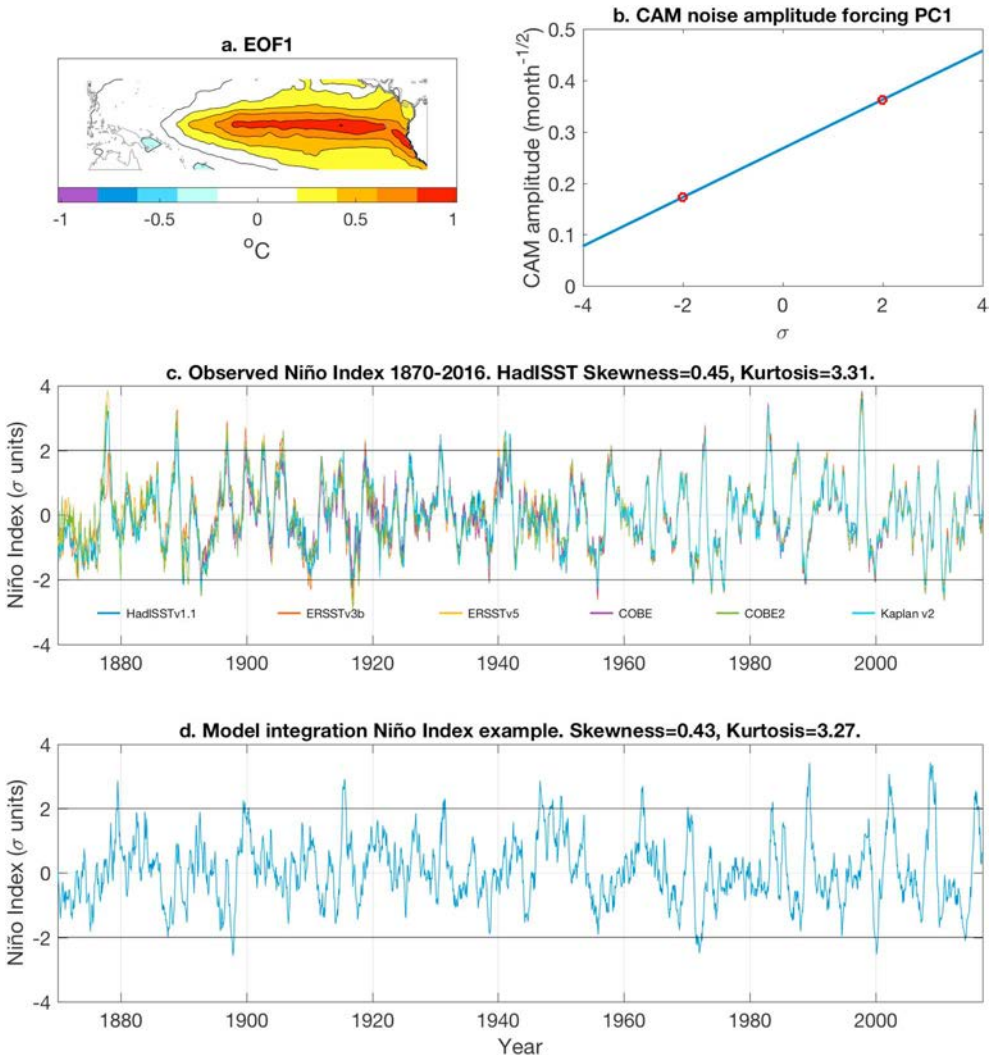

Figure 1. (a) HadISST v1.1 Tropical Pacific (1870–2016) first EOF of monthly sea surface temperature anomalies. (b) CAM noise amplitude in units of standard deviation $\sigma^{-1}(G_1 + E_1 PC1)$, with σ denoting PC1 (the Niño index) standard deviation. The red circles show the CAM noise amplitude for -2σ and $+2\sigma$ anomalies. (c) Niño index time series for the six different data sets considered. (d) Niño index time series taken from a 147-year epoch from the CAM-Linear Inverse Model integration. EOF = Empirical Orthogonal Function; CAM = correlated additive-multiplicative; PC = principal component.

cover approximately the last 150 years, similar lengthy data sets of ocean heat content measures are unavailable. To test reconstruction uncertainty, we consider six data sets (Hirahara et al., 2014; Huang et al., 2017; Ishii et al., 2005; Kaplan et al., 1998; Rayner et al., 2003; Smith et al., 2008; see supporting information Table S1). From each, we construct LIMs using the first 15 principal components (PCs) of monthly SST anomalies (accounting for 90% of the SST variance in the HadISST v1.1 data set) calculated in the region 20°S–20°N, 120°E–70°W. Anomalies are calculated by first subtracting the long-term annual mean SSTs at each grid point, then a nonlinear trend during the period considered is removed by a fourth-order polynomial, and the seasonal cycle is removed by subtracting the first four annual Fourier harmonics. Removing the nonlinear trend eliminates the PC most associated with linear trends in the 1950–2010 period (L'Heureux et al., 2013), so that the leading two Empirical Orthogonal Functions (EOFs) correspond to the familiar EOF1–EOF2 pair from many previous studies (e.g., Ashok et al., 2007; Capotondi & Sardeshmukh, 2015; Karamperidou et al., 2017; Takahashi et al., 2011; Thomas et al., 2018; Vimont et al., 2014).

Results from the different data sets are generally consistent, so we display results only from HadISST v1.1, covering 1870–2016. Figure 1a shows the familiar EOF1 spatial pattern (Figure S1 shows EOF2 and EOF3

spatial patterns). We call the associated standardized PC1 the Niño index (Figure 1c), since its correlation coefficient with Niño3.4 is 0.97.

Standard LIM (1) and CAM-LIM (2) parameters are calculated following PS95 and M18, respectively, for each individual data set. As in other methods to estimate state-dependent noise from data (cf. Levine & Jin, 2017), we first determine the predictable dynamical operator **M**, which in this study provides a good representation of the evolution of the system up to 15 months in advance for the HadISST v1.1 data set, although this particular aspect is sensitive to the data set used (Text S1). The SST-only LIM implicitly assumes that deterministic wind and thermocline anomalies may be expressed in terms of SST anomalies at monthly time scales (Neelin, 1991; PS95). This misses some dynamics associated with recharge-discharge processes (Jin, 1997; Neelin et al., 1998) out of equilibrium with SSTs, which extends the memory of the system (Johnson et al., 2000; Newman et al., 2011; Xue et al., 2000).

In general, $\mathbf{B^M}$ in (2) includes local and nonlocal state-dependent noise sources as well as covariance between different CAM noise processes (cf. Majda et al., 2008; SS09), all interactions that are unlikely to be resolved by even the long SST time series considered here. For this reason, as well as the lack of estimation methods for more complex CAM noise formulations, we consider a restricted "diagonal" form of $\mathbf{B^M}$ driving PC_i as follows:

$$\begin{aligned} B^M_{ij} &= (G_i + E_i x_i)\delta_{ij}, \quad i = 1, 2, 3. \\ B^M_{ij} &= 0, \quad i \geq 4. \end{aligned} \tag{3}$$

This formulation captures asymmetries in noise amplitude along each PC direction. Note that if $G_i \neq 0$, the CAM noise amplitude is different for positive and negative anomalies. To reduce the number of parameters to be determined, CAM noise is assumed to involve only the first three PCs, since these exhibit the largest asymmetry in probability distribution and have skewness that are not accounted for by the (1) standard LIM (Figure S2; in addition, PCs 6, 8, 13, and 15 exhibit smaller but significant deviations). Further details of the M18 methodology are given in Text S2. Tests of the methodology self-consistency and a discussion of its limitations are given in Text S3 (see also M18). We note that this CAM-LIM yields only modest improvements over the standard LIM in the representation of the joint PC1-PC2 probability (not shown). Improvement of this aspect likely needs a more complete CAM noise representation or deterministic nonlinearity (Takahashi et al., 2018), and investigation of it is deferred for future research.

Each LIM (equations (1) and (2)) is then integrated forward 200,000 years using the Heun stochastic integration method (Ewald & Penland, 2009; Rümelin, 1982) with a time step of 3 hr; then monthly output is sampled. Deviations from Gaussianity in observed and modeled time series, represented by a centered variable x, are determined by the sample skewness $S = \frac{\langle x^3 \rangle}{\langle x^2 \rangle^{3/2}}$ and sample kurtosis $K = \frac{\langle x^4 \rangle}{\langle x^2 \rangle^2}$ (Joanes & Gill, 1998). Skewness measures the degree of asymmetry with respect to the mean of the distribution ($S = 0$ for a Gaussian), and kurtosis provides information on the heaviness of the tails, with $K > 3$ ($K = 3$ for a Gaussian) indicating a larger proportion of extreme events compared to a Gaussian of the same standard deviation. Confidence intervals (5th–95th percentile) of CAM-LIM generated statistics are calculated by dividing the full integration onto 1,360 nonoverlapping realizations or *epochs* of 147 years length (the length of the HadISST data set).

3. Results

3.1. EN-LN Asymmetry in Amplitude

Figure 1b shows the CAM noise amplitude ($G_1 + E_1 PC1$) as a function of the Niño index PC1 (in standardized units), calculated from the HadISST v1.1 data set. Since $G_1 > 0$, the overall noise amplitude is stronger for EN events compared to LN events, in agreement with other estimates (Capotondi et al., 2018; Kug et al., 2008). For example, the CAM noise amplitude for a positive Niño index anomaly of 2 standard deviations σ is approximately twice the CAM noise amplitude for a -2σ anomaly. The CAM noise amplitude has some quantitative sensitivity to a number of data preprocessing choices (number of EOFs retained and lag used to calculate the LIM and different detrending options) and to geographical region, but in all cases the CAM noise amplitude is similar and yields a long-term positively skewed Niño index (see Figure S6 and Text S4).

To illustrate the effect of noise amplitude asymmetry on the resulting EN and LN amplitudes, Figure 1d shows the Niño index time series taken from a 147-year epoch of the CAM-LIM integration, which can

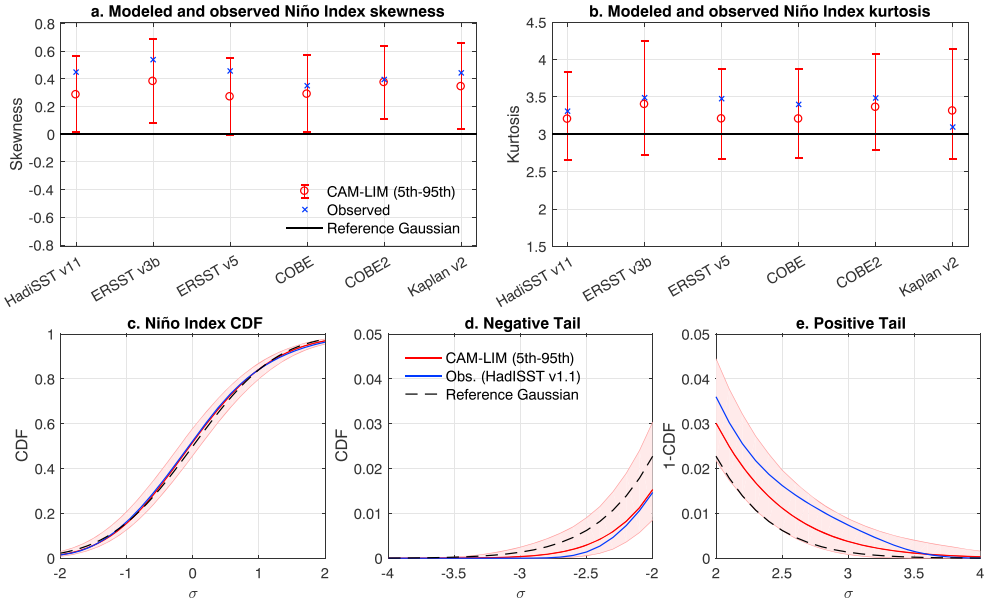

Figure 2. (a,b) Observed and modeled Niño index skewness (kurtosis). In each panel, the error bars (5th–95th) are centered on the skewness (kurtosis) calculated from the full CAM-LIM integration. (c) Observed and modeled CDF of the Niño index over its central range (-2σ to 2σ). (d) Similar to (c) but showing the negative tail (-4σ to -2σ). (e) Similar to (c) but showing the positive tail ($+2\sigma$ to $+4\sigma$). In the last case, the exceedance (1-CDF) is shown instead. A Gaussian CDF is also plotted for reference. The solid red line represents the estimate from the full integration and shading the 5th–95th percentile calculated from estimations in each 147-year epoch. CAM = correlated additive-multiplicative; LIM = Linear Inverse Model; CDF = cumulative density function.

be compared to observations (Figure 1c). The pattern of growth and decay of this index is consistent with observations, with similar skewness and kurtosis, and larger extreme EN compared to LN events.

The extended model integration allows assessment of multidecadal-centennial changes in ENSO variability generated by (2), and its corresponding confidence intervals. For each data set, the observed positive skewness (Figure 2a) and kurtosis (Figure 2b) of the Niño index are well within the 5th–95th percentile of CAM-LIM realizations but not within the 5th–95th percentile of the standard LIM (Figure S2), showing that only the CAM-LIM (2) captures observed EN-LN amplitude asymmetry. The spread of skewness values calculated from each 147-year epoch implies that different realizations have a wide variation in the degree of ENSO asymmetry that are all consistent with the CAM-noise process (2). The spread in kurtosis shows that while most realizations generate more extreme events compared to a Gaussian process, there are a significant number of 147-year epochs with fewer extremes.

Figures 2c–2e compare the observed and modeled Niño index cumulative density function. (Similar plots for PC2 and PC3 indices are shown in Figures S7 and S8.) Both the standard LIM (Figure S9) and CAM-LIM (Figure 2c) generate a cumulative density function consistent with observations within the central range of anomaly amplitudes $[-2\sigma, 2\sigma]$, although even in this range the CAM-LIM fit is visually better. At the extreme negative (less than -2σ; Figure 2d) and positive (greater than 2σ; Figure 2e) tails, the observed amplitude asymmetry is much better matched by the CAM-LIM: The standard LIM overestimates the probability of strong LN events and underestimates the probability of extreme EN events (Figure S9), while the CAM-LIM generates fewer extreme LN events and more strong EN events. For example, CAM-LIM generates a median of 53 (27) months of extreme EN (LN) events (Niño index magnitude $> 2\sigma$), which compares well with the observed 55 (23) months in HadISST v1.1.

3.2. EN-LN Asymmetry in Event Duration

As discussed in section 1, observed LN events are typically (but not always) more persistent than EN events (DiNezio & Deser, 2014; Ohba & Ueda, 2009; Ohba, 2013; Okumura & Deser, 2010; Okumura et al., 2017). For this analysis, we define EN (LN) events as those consisting of three or more consecutive months with Niño index value $> H$ (less than $-H$), where H represents some threshold amplitude. We find that observed EN-LN duration asymmetry is sensitive to the value of H, a new result to which we will return below, so we conduct

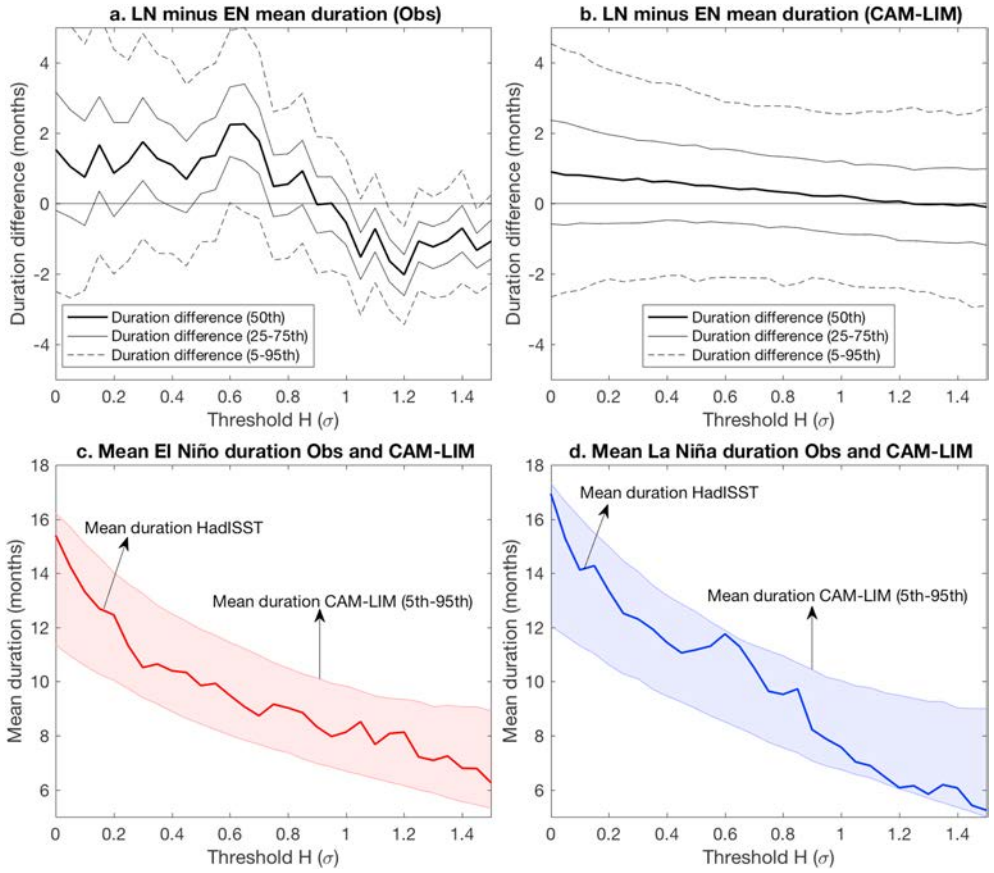

Figure 3. (a) Observed (HadISST v1.1) difference in mean LN and EN duration as a function of threshold used to define events. The solid line shows the 50th percentile of this difference calculated by using a bootstrap with replacement procedure (Efron & Tibshirani, 1994), under the assumption of independence of events. Confidence intervals (25th–75th and 5th–95th) are calculated similarly. (b) Mean LN and EN duration generated by CAM-LIM as a function of threshold used to define events. Confidence intervals and median duration difference are calculated from 1,367 epochs of 147 years contained within the full CAM-LIM integration. (c,d) Mean observed EN (LN) duration as a function of threshold (solid) and range (5th-95th) of mean EN (LN) duration calculated by Monte-Carlo sampling of epochs within the full CAM-LIM integration. EN = El Niño; LN = La Niña; CAM = correlated additive-multiplicative; LIM = Linear Inverse Model.

our analysis for H ranging from 0 to 1.5 Niño index standard deviation σ. Note that $H = 0.65\sigma$ corresponds approximately to a Niño3.4 index of 0.5 °C. Due to the small number of ENSO events in the HadISST v1.1 data set (with fewer than 80 events for $H = 0.65\sigma$), statements based on the observed distribution of EN and LN durations cannot be made with any useful level of uncertainty, so here we concentrate on the mean duration.

Figure 3a shows the observed LN-EN asymmetry in mean event duration. Likely due to the small number of events, this observed asymmetry, whose uncertainty is estimated here using a bootstrap with replacement procedure (Efron & Tibshirani, 1994), cannot be ascertained with a high degree of confidence (Figure 3a), although it has also been found in models (DiNezio & Deser, 2014). A key feature of the observed event duration asymmetry seen in Figure 3a is its dependence on threshold H: Observed LN events persist for longer than EN events on average only if events are defined by $H < 0.9\sigma$. However, when events are defined for $H > 0.9\sigma$, then EN events actually tend to last longer. Similar behavior is also seen in the model, except that this transition occurs for $H \sim 1.2\sigma$ (Figure 3b). We note in this case that due to the large number of epochs simulated by the CAM-LIM, the duration asymmetry (and confidence interval; Figure 3b) is smoother, and also typically less asymmetric, than that of the relatively short observational record (Figure 3a). However, individual epochs may exhibit asymmetry in persistence as strong or stronger than in observations.

Observed event durations, as a function of threshold H, lie well within the 5th–95th percentile bounds for both the mean EN (Figure 3c) and LN (Figure 3d) distributions generated by the full CAM-LIM integration.

That is, the CAM-LIM provides a plausible explanation for the observed asymmetry in persistence, and its dependence on the observed threshold, at this confidence level. For example, when using $H = 0.4\sigma$ to define events, the observed mean EN duration of 10.4 months corresponds to the 44th percentile, and the observed mean LN duration of 11.5 months corresponds to the 62nd percentile of their respective modeled distributions. In this case two thirds of epochs have LN events lasting longer than EN events on average, and 87% of epochs have a longer than 10 months mean LN duration, as opposed to 67.5% for EN.

SCP15 noted that linear dynamical systems forced by CAM noise have skewed and heavy-tailed distributions with many distinctive features. In particular, in such a system the duration of positive and negative events is asymmetric but varies in a way that specifically depends upon event amplitude, which they showed can be a direct result of the interaction between linear dynamics and noise with asymmetric amplitude. For a given amplitude, a positive anomaly is more likely than a negative anomaly to be disrupted by noise, since on average, it experiences larger noise events (Figure 1b). If the noise acts to reduce the size of the positive anomaly, it will then be less likely for subsequent (weaker) noise to return it to its original scale. The same argument with reversed polarity explains the enhanced duration of LN events. That is, it is not noise that makes LN events more likely to persist but rather the relative *absence* of noise. Thus, for low-threshold exceedance, LN events are more persistent than EN events. However, the stronger noise also means the potential for larger events, leading to the observed amplitude asymmetry (section 3.1). For larger threshold exceedance, the noise is acting against larger tendencies due to deterministic damping. Thus, the weaker noise forcing at negative values (LN events) is less likely to maintain such anomalies against dissipation (see Sura et al., 2005), leading to more persistent EN events than LN events in this case.

4. Discussion

We apply an extension of the LIM technique, called the CAM-LIM (M18), where the stochastic forcing includes a linearly state-dependent asymmetric component, to empirically model the dynamics of monthly Tropical Pacific SST anomalies. State-dependent noise sources are represented by a simple CAM noise parameterization (SS09), which can capture asymmetries in the noise response to the background SST state (as it may be expected from WWBs interacting with ENSO, e.g., see below), that may generate skewed and also heavy-tailed distributions (Penland & Sardeshmukh, 2012) and asymmetries in event duration (SCP15). We find that this state-dependent noise is sufficient, without invoking deterministic nonlinearity, to generate asymmetry in amplitude between EN and LN states generally consistent with observations, in agreement with the conceptual model of ENSO-WWBs interaction of Levine et al. (2016) and Levine and Jin (2017). Additionally, this dynamical system also generates LN events that are on average more persistent than EN events, in a manner consistent (at the 5th–95th percentile confidence interval) with a corresponding analysis of observed ENSO events. Consequently, this framework provides a plausible *null hypothesis* for EN-LN asymmetry and implies that this asymmetry is not *necessarily* a salient feature of deterministic nonlinear dynamics.

In addition to evaluating the extent to which the observed EN-LN asymmetry may be consistent with deterministically linear dynamics, CAM-LIM (2) may also be used to assess the statistical significance of multidecadal changes of Niño index statistics. Our CAM-LIM results show a substantial range in measures of non-Gaussianity, when evaluated across epochs of length comparable to the HadISST data set, all consistent with the same CAM-LIM generative process (2). This has important consequences for hypothesis testing of ENSO extremes (Newman et al., 2018; SCP15) and highlights the need for long data sets to adequately constrain observational estimates of ENSO asymmetries, consistent with Wittenberg (2009). This also suggests that observed changes in the Niño index PDF over the recent decades are not necessarily indicative of changes in the underlying Tropical Pacific dynamics (cf. Hu & Fedorov, 2018; Rodrigues et al., 2019), since they could occur from sampling variability.

The short-time scale feedback between SSTs and WWBs (Eisenman et al., 2005; Gebbie et al., 2007; Lengaigne et al., 2004; Lopez et al., 2013; Puy et al., 2016; Vecchi & Harrison, 2000) is asymmetric, since it occurs when increases in Central/Western Tropical Pacific SSTs lead to increases in WWBs, which forces an ocean response that further increases SSTs. A version of this feedback may be captured by CAM-LIM: an increase of SSTs projecting onto EOF1 drives an increase in CAM noise amplitude, which for persistent noise realizations (which might represent WWBs in the model), increases the likelihood of a larger SST increase, which then completes the loop by increasing the CAM noise amplitude. Easterly wind bursts

would be disfavored by this CAM noise forcing, as they lead to a reduction of CAM noise amplitude. Note that this feedback loop is not deterministic and, as a consequence, has a larger unpredictable component. Previous studies have modeled WWBs based on a SST threshold for convection (e.g., Christensen et al., 2017; Levine et al., 2016). In reality, the relation between SST and convection is indirect: Convection is triggered by high values of column water vapor, and the *probability* of high water vapor occurrence increases for high SSTs (Neelin et al., 2009). This renders the pickup of convection with SST smoother than a strict threshold. If indeed most of the state-dependent noise in the PC1 direction results from WWBs, then the CAM noise amplitude (Figure 1b) could be regarded as an approximation to these processes.

Whether deterministic nonlinearity or state-dependent noise is the main contributor to EN-LN asymmetry has important consequences for predictability of the strongest EN events (as well as for prospects of LN long-term predictability, see DiNezio, Deser, Karspeck et al., 2017; DiNezio, Deser, Okumura, et al., 2017). If this asymmetry is largely deterministic, then finding the right balance of processes in climate models may improve estimates of predictability of the largest events, which is currently a deficiency in these models (Barnston et al., 2017; L'Heureux et al., 2017). If the deterministic dynamics are close to linear and the asymmetry is generated due to rapidly decorrelating unresolved nonlinear processes, then the prospects of predictability of these events is compromised; however, incorporation of state-dependent noise would improve an ensemble (probabilistic) forecast by better characterizing the range of possible outcomes. Evidence for the role of state-dependent noise in generating the asymmetry may be found in the similar skill that linear and nonlinear inverse models in the Niño3.4 area have (Chen et al., 2016), as well as further evidence suggesting that at seasonal time scales, the Tropical Pacific forecast skill is very close to linear, except perhaps in the far eastern Pacific (Ding et al., 2018; Newman & Sardeshmukh, 2017). In this case, further model development may not significantly improve the forecast skill of the largest EN events beyond what can be explained by a linear system forced by CAM noise.

Acknowledgments
This work was supported by National Science Foundation Grants AGS-1463643 and AGS-1463970 (C. M., M. N., and D. J. V.) and National Science Foundation Grant AGS-1540518 (C. M. and J. D. N.). The sea surface temperature datasets used in this paper are publicly available in websites listed in Table S1.

References

An, S.-I., & Jin, F.-F. (2004). Nonlinearity and asymmetry of ENSO*. *Journal of Climate*, *17*, 2399–2412. https://doi.org/10.1175/1520-0442(2004)017h2399:NAAOEi2.0.CO;2

Ashok, K., Behera, S. K., Rao, S. A., Weng, H., & Yamagata, T. (2007). El Niño Modoki and its possible teleconnection. *Journal of Geophysical Research*, *112*, C11007. https://doi.org/10.1029/2006JC003798

Ault, T. R., Deser, C., Newman, M., & Emile-Geay, J. (2013). Characterizing decadal to centennial variability in the equatorial Pacific during the last millennium. *Geophysical Research Letters*, *40*, 3450–3456. https://doi.org/10.1002/grl.50647

Barnston, A. G., Tippett, M. K., Ranganathan, M., & L'Heureux, M. L. (2017). Deterministic skill of ENSO predictions from the North American Multimodel Ensemble. *Climate Dynamics*, 1–20. https://doi.org/10.1007/s00382-017-3603-3

Bianucci, M., Capotondi, A., Mannella, R., & Merlino, S. (2018). Linear or nonlinear modeling for ENSO dynamics? *Atmosphere*, *9*, 435. https://doi.org/10.3390/atmos9110435

Blanke, B., Neelin, J. D., & Gutzler, D. (1997). Estimating the effect of stochastic wind stress forcing on ENSO irregularity. *Journal of Climate*, *10*(7), 1473–1486. https://doi.org/10.1175/1520-0442(1997)010h1473:ETEOSWi2.0.CO;2

Burgers, G., & Stephenson, D. B. (1999). The normality of El Niño. *Geophysical Research Letters*, *26*, 1027–1030. https://doi.org/10.1029/1999GL900161

Capotondi, A., & Sardeshmukh, P. D. (2015). Optimal precursors of different types of ENSO events. *Geophysical Research Letters*, *42*, 9952–9960. https://doi.org/10.1002/2015GL066171

Capotondi, A., Sardeshmukh, P. D., & Ricciardulli, L. (2018). The nature of the stochastic wind forcing of ENSO. *Journal of Climate*, *31*(19), 8081–8099. https://doi.org/10.1175/JCLI-D-17-0842.1

Chekroun, M. D., Neelin, JD., Kondrashov, D., McWilliams, J. C., & Ghil, M. (2014). Rough parameter dependence in climate models and the role of Ruelle-Pollicott resonances. *Proceedings of the National Academy of Sciences of the United States of America*, *111*(5), 1684–1690. https://doi.org/10.1073/pnas.1321816111

Chen, C., Cane, M. A., Henderson, N., Lee, D. E., Chapman, D., Kondrashov, D., & Chekroun, M. D. (2016). Diversity, nonlinearity, seasonality, and memory effect in ENSO simulation and prediction using empirical model reduction. *Journal of Climate*, *29*(5), 1809–1830. https://doi.org/10.1175/JCLI-D-15-0372.1

Christensen, H. M., Berner, J., Coleman, DanielleR. B., & Palmer, T. N. (2017). Stochastic parameterization and El Niño Southern Oscillation. *Journal of Climate*, *30*, 17–38. https://doi.org/10.1175/JCLI-D-16-0122.1

DiNezio, P. N., & Deser, C. (2014). Nonlinear controls on the persistence of La Niña*. *Journal of Climate*, *27*(19), 7335–7355. https://doi.org/10.1175/JCLI-D-14-00033.1

DiNezio, P. N., Deser, C., Karspeck, A., Yeager, S., Okumura, Y., Danabasoglu, G., et al. (2017). A 2 year forecast for a 60% chance of La Niña in 2017–2018. *Geophysical Research Letters*, *44*, 11,624–11,635. https://doi.org/10.1002/2017GL074904

DiNezio, P. N., Deser, C., Okumura, Y., & Karspeck, A. (2017). Predictability of 2-year La Niña events in a coupled general circulation model. *Climate Dynamics*, *49*(11-12), 4237–4261. https://doi.org/10.1007/432s00382-017-3575-3

Ding, H., Newman, M., Alexander, M. A., & Wittenberg, A. T. (2018). Skillful climate forecasts of the tropical Indo-Pacific Ocean using model-analogs. *Journal of Climate*, *31*(14), 5437–5459. https://doi.org/10.1175/JCLI-D-17-0661.1

Dong, B. (2005). Asymmetry between El Niño and La Niña in a global coupled GCM with an eddy-permitting ocean resolution. *Journal of Climate*, *18*(16), 3373–3387. https://doi.org/10.1175/JCLI3454.1

Efron, B., & Tibshirani, R. (1994). An introduction to the bootstrap, Chapman & Hall.

Eisenman, I., Yu, L., & Tziperman, E. (2005). Westerly wind bursts: ENSO's tail rather than the dog? *Journal of Climate*, *18*(24), 5224–5238.
Ewald, B., & Penland, C. (2009). Numerical generation of stochastic differential equations in climate models, *Handbook of numerical analysis* (Vol. 14, pp. 279–306). Amsterdam: Elsevier. https://doi.org/10.1016/S1570-8659(08)00206-8
Gebbie, G., Eisenman, I., Wittenberg, A., & Tziperman, E. (2007). Modulation of westerly wind bursts by sea surface temperature: A semistochastic feedback for ENSO. *Journal of the Atmospheric Sciences*, *64*(9), 3281–3295. https://doi.org/10.1175/JAS4029.1
Hasselmann, K. (1976). Stochastic climate models. Part I. Theory. *Tellus*, *28*(6), 473–485. https://doi.org/10.1111/j.2153-3490.1976.tb00696.x
Hirahara, S., Ishii, M., & Fukuda, Y. (2014). Centennial-scale sea surface temperature analysis and its uncertainty. *Journal of Climate*, *27*(1), 57–75. https://doi.org/10.1175/JCLI-D-12-00837.1
Hu, S., & Fedorov, A. V. (2018). Cross-equatorial winds control El Niño diversity and change. *Nature Climate Change*, *8*(9), 798–802. https://doi.org/10.1038/s41558-018-0248-0
Hu, Z.-Z., Kumar, A., Xue, Y., & Jha, B. (2014). Why were some La Niñas followed by another La Niña? *Climate Dynamics*, *42*(3-4), 1029–1042. https://doi.org/10.1007/s00382-013-1917-3
Huang, B., Thorne, P. W., Banzon, V. F., Boyer, T., Chepurin, G., Lawrimore, J. H., et al. (2017). Extended Reconstructed Sea Surface Temperature, Version 5 (ERSSTv5): Upgrades, validations, and intercomparisons. *Journal of Climate*, *30*(20), 8179–8205. https://doi.org/10.1175/JCLI-D-16-0836.1
Im, S.-H., An, S.-I., Kim, S. T., & Jin, F.-F. (2015). Feedback processes responsible for El Niño-La Niña amplitude asymmetry. *Geophysical Research Letters*, *42*, 5556–5563. https://doi.org/10.1002/2015GL064853
Ishii, M., Shouji, A., Sugimoto, S., & Matsumoto, T. (2005). Objective analyses of sea-surface temperature and marine meteorological variables for the 20th century using ICOADS and the Kobe Collection. *International Journal of Climatology*, *25*(7), 865–879. https://doi.org/10.1002/joc.1169
Jin, F.-F. (1997). An equatorial ocean recharge paradigm for ENSO. Part I: Conceptual model. *Journal of the Atmospheric Sciences*, *54*(7), 811–829. https://doi.org/10.1175/1520-0469(1997)054h0811:AEORPFi2.0.CO;2
Jin, F.-F., An, S., Timmermann, A., & Zhao, J. (2003). Strong El Niño events and nonlinear dynamical heating. *Geophysical Research Letters*, *30*(3), 1120. https://doi.org/10.1029/2002GL016356
Jin, F.-F., Lin, L., Timmermann, A., & Zhao, J. (2007). Ensemble-mean dynamics of the ENSO recharge oscillator under state-dependent stochastic forcing. *Geophysical Research Letters*, *34*, L03807. https://doi.org/10.1029/2006GL027372
Jin, F.-F., Neelin, J. D., & Ghil, M. (1994). El Nino on the devil's staircase: Annual subharmonic steps to chaos. *Science*, *264*(5155), 70–72. https://doi.org/10.1126/science.264.5155.70
Joanes, D. N., & Gill, C. A. (1998). Comparing measures of sample skewness and kurtosis. *Journal of the Royal Statistical Society Series D: The Statistician*, *47*, 183–189. https://doi.org/10.1111/4871467-9884.00122
Johnson, S. D., Battisti, D. S., & Sarachik, E. S. (2000). Empirically derived Markov models and prediction of tropical Pacific sea surface temperature anomalies*. *Journal of Climate*, *13*(1), 3–17. https://doi.org/10.1175/1520-0442(2000)013h0003:EDMMAPi2.0.CO;2
Kang, I.-S., & Kug, J.-S. (2002). El Niño and La Niña sea surface temperature anomalies: Asymmetry characteristics associated with their wind stress anomalies. *Journal of Geophysical Research*, *107*(D19), 4372. https://doi.org/10.1029/2001JD000393
Kaplan, A., Cane, M. A., Kushnir, Y., Clement, A. C., Blumenthal, M. B., & Rajagopalan, B. (1998). Analyses of global sea surface temperature 1856-1991. *Journal of Geophysical Research*, *103*, 18,567–18,589. https://doi.org/10.1029/97JC01736
Kapur, A., & Zhang, C. (2012). Multiplicative MJO forcing of ENSO. *Journal of Climate*, *25*(23), 8132–8147. https://doi.org/10.1175/JCLI-D-11-00609.1
Karamperidou, C., Jin, F.-F., & Conroy, J. L. (2017). The importance of ENSO nonlinearities in tropical Pacific response to external forcing. *Climate Dynamics*, *49*(7-8), 2695–2704. https://doi.org/10.1007/s00382-016-3475-y
Kleeman, R., & Moore, A. M. (1997). A theory for the limitation of ENSO predictability due to stochastic atmospheric transients. *Journal of the Atmospheric Sciences*, *54*(6), 753–767. https://doi.org/10.1175/1520-0469(1997)054h0753:ATFTLOi2.0.CO;2
Kondrashov, D., Kravtsov, S., Robertson, A. W., & Ghil, M. (2005). A hierarchy of data-based ENSO models. *Journal of Climate*, *18*(21), 4425–4444. https://doi.org/10.1175/JCLI3567.1
Kug, J.-S., Jin, F.-F., Sooraj, K. P., & Kang, I.-S. (2008). State-dependent atmospheric noise associated with ENSO. *Geophysical Research Letters*, *35*, L05701. https://doi.org/10.1029/2007GL032017
L'Heureux, M. L., Collins, D. C., & Hu, Z.-Z. (2013). Linear trends in sea surface temperature of the tropical Pacific Ocean and implications for the El Niño-Southern Oscillation. *Climate Dynamics*, *40*(5-6), 1223–1236. https://doi.org/10.1007/s00382-012-1331-2
L'Heureux, M. L., Takahashi, K., Watkins, A. B., Barnston, A. G., Becker, E. J., Di Liberto, T. E., et al. (2017). Observing and predicting the 2015/16 El Niño. *Bulletin of the American Meteorological Society*, *98*(7), 1363–1382. https://doi.org/10.1175/BAMS-D-16-0009.1
Lengaigne, M., Guilyardi, E., Boulanger, J.-P., Menkes, C., Delecluse, P., Inness, P., et al. (2004). Triggering of El Niño by westerly wind events in a coupled general circulation model. *Climate Dynamics*, *23*(6), 601–620. https://doi.org/10.1007/s00382-004-0457-2
Levine, A., & Jin, F. F. (2017). A simple approach to quantifying the noise ENSO interaction. Part I: Deducing the state-dependency of the windstress forcing using monthly mean data. *Climate Dynamics*, *48*(1-2), 1–18. https://doi.org/10.1007/s00382-015-2748-1
Levine, A., Jin, F. F., & McPhaden, M. J. (2016). Extreme noise–extreme El Niño: How state-dependent noise forcing creates El Niño–La Niña asymmetry. *Journal of Climate*, *29*(15), 5483–5499. https://doi.org/10.1175/JCLI-D-16-0091.1
Liang, J., Yang, X.-Q., & Sun, D.-Z. (2012). The effect of ENSO events on the tropical Pacific mean climate: Insights from an analytical model. *Journal of Climate*, *25*(21), 7590–7606. https://doi.org/10.1175/JCLI-D-11-00490.1
Lopez, H., Kirtman, B. P., Tziperman, E., & Gebbie, G. (2013). Impact of interactive westerly wind bursts on CCSM3. *Dynamics of Atmospheres and Oceans*, *59*, 24–51. https://doi.org/10.1016/J.DYNATMOCE.2012.11.001
Majda, A. J., Franzke, C., & Khouider, B. (2008). An applied mathematics perspective on stochastic modelling for climate. *Philosophical transactions. Series A, Mathematical, physical, and engineering sciences*, *366*(1875), 2429–55. https://doi.org/10.1098/rsta.2008.0012
Martinez-Villalobos, C. (2016). Deterministic and stochastic models of tropical climate variability (PhD thesis), University of Wisconsin-Madison.
Martinez-Villalobos, C., Vimont, D. J., Penland, C., Newman, M., & Neelin, J. David (2018). Calculating state-dependent noise in a linear inverse model framework. *Journal of the Atmospheric Sciences*, *75*(2), 479–496. https://doi.org/10.1175/JAS-D-17-0235.1
Meinen, C. S., & McPhaden, M. J. (2000). Observations of warm water volume changes in the equatorial Pacific and their relationship to El Niño and La Niña. *Journal of Climate*, *13*(20), 3551–3559. https://doi.org/10.1175/1520-0442(2000)013h3551:OOWWVCi2.0.CO;2
Neelin, J. D. (1991). The slow sea surface temperature mode and the fast-wave limit: Analytic theory for tropical interannual oscillations and experiments in a hybrid coupled model. *Journal of the Atmospheric Sciences*, *48*(4), 584–606. https://doi.org/10.1175/1520-0469(1991)048h0584:TSSSTMi2.0.CO;2
Neelin, J. D., Battisti, D. S., Hirst, A. C., Jin, F.-F., Wakata, Y., Yamagata, T., & Zebiak, S. E. (1998). ENSO theory. *Journal of Geophysical Research*, *103*, 14,261–14,290. https://doi.org/10.1029/97JC03424

Neelin, J. D., Peters, O., & Hales, K. (2009). The transition to strong convection. *Journal of the Atmospheric Sciences*, *66*(8), 2367–2384. https://doi.org/10.1175/2009JAS2962.1

Newman, M., Alexander, M. A., & Scott, J. D. (2011). An empirical model of tropical ocean dynamics. *Climate Dynamics*, *37*(9-10), 1823–1841. https://doi.org/10.1007/s00382-011-1034-0

Newman, M., & Sardeshmukh, P. D. (2017). Are we near the predictability limit of tropical Indo-Pacific sea surface temperatures? *Geophysical Research Letters*, *44*, 8520–8529. https://doi.org/10.1002/2017GL074088

Newman, M., Sardeshmukh, P. D., & Penland, C. (2009). How important is air–sea coupling in ENSO and MJO evolution? *Journal of Climate*, *22*(11), 2958–2977. https://doi.org/10.1175/2008JCLI2659.1

Newman, M., Wittenberg, A. T., Cheng, L., Compo, G. P., & Smith, C. A. (2018). The extreme 2015/16 El Niño, in the context of historical climate variability and change. *Bulletin of the American Meteorological Society*, *99*(1), S16–S20. https://doi.org/10.1175/BAMS-D-17-0116.1

Ohba, M. (2013). Important factors for long-term change in ENSO transitivity. *International Journal of Climatology*, *33*(6), 1495–1509. https://doi.org/10.1002/joc.3529

Ohba, M., Nohara, D., & Ueda, H. (2010). Simulation of asymmetric ENSO transition in WCRP CMIP3 multimodel experiments. *Journal of Climate*, *23*(22), 6051–6067. https://doi.org/10.1175/2010JCLI3608.1

Ohba, M., & Ueda, H. (2009). Role of nonlinear atmospheric response to SST on the asymmetric transition process of ENSO. *Journal of Climate*, *22*(1), 177–192. https://doi.org/10.1175/2008JCLI2334.1

Ohba, M., & Watanabe, M. (2012). Role of the indo-pacific interbasin coupling in predicting asymmetric ENSO transition and duration. *Journal of Climate*, *25*(9), 3321–3335. https://doi.org/10.1175/JCLI-D-11-00409.1

Okumura, Y. M., & Deser, C. (2010). Asymmetry in the duration of El Niño and La Niña. *Journal of Climate*, *23*(21), 5826–5843. https://doi.org/10.1175/2010JCLI3592.1

Okumura, Y. M., Sun, T., & Wu, X. (2017). Asymmetric modulation of El Niño and La Niña and the linkage to tropical Pacific decadal variability. *Journal of Climate*, *30*(12), 4705–4733. https://doi.org/10.1175/597JCLI-D-16-0680.1

Penland, C. (1996). A stochastic model of IndoPacific sea surface temperature anomalies. *Physica D: Nonlinear Phenomena*, *98*(2-4), 534–558. https://doi.org/10.1016/0167-2789(96)00124-8

Penland, C. (2010). A linear stochastic model of tropical sea surface temperatures related to El Niño. *American Geophysical Union (AGU)*, *189*, 65–77. https://doi.org/10.1029/2008GM000814

Penland, C., & Sardeshmukh, P. D. (1995). The optimal growth of tropical sea surface temperature anomalies. *Journal of Climate*, *8*(8), 1999–2024. https://doi.org/10.1175/1520-0442(1995)008h1999:TOGOTSi2.0.CO;2

Penland, C., & Sardeshmukh, P. D. (2012). Alternative interpretations of power-law distributions found in nature. *Chaos: An Interdisciplinary Journal of Nonlinear Science*, *22*(2), 23119. https://doi.org/10.1063/1.4706504

Perez, C. L., Moore, A. M., Zavala-Garay, J., & Kleeman, R. (2005). A comparison of the influence of additive and multiplicative stochastic forcing on a coupled model of ENSO. *Journal of Climate*, *18*(23), 5066–5085. https://doi.org/10.1175/JCLI3596.1

Puy, M., Vialard, J., Lengaigne, M., & Guilyardi, E. (2016). Modulation of equatorial Pacific westerly/easterly wind events by the Madden–Julian oscillation and convectively-coupled Rossby waves. *Climate Dynamics*, *46*(7-8), 2155–2178. https://doi.org/10.1007/s00382-015-2695-x

Rayner, N. A., Parker, D. E., Horton, E. B., Folland, C. K., Alexander, L. V., Rowell, D. P., et al. (2003). Global analyses of sea surface temperature, sea ice, and night marine air temperature since the late nineteenth century. *Journal of Geophysical Research*, *108*(D14), 4407. https://doi.org/10.1029/2002JD002670

Rodrigues, R. R., Subramanian, A., Zanna, L., & Berner, J. (2019). ENSO bimodality and extremes. *Geophysical Research Letters*, *46*, 4883–4893. https://doi.org/10.1029/2019GL082270

Rümelin, W. (1982). Numerical treatment of stochastic differential equations. *SIAM Journal on Numerical Analysis*, *19*(3), 604–613. https://doi.org/10.1137/0719041

Sardeshmukh, P. D., Compo, G. P., & Penland, C. (2015). Need for caution in interpreting extreme weather statistics. *Journal of Climate*, *28*(23), 9166–9187. https://doi.org/10.1175/JCLI-D-15-0020.1

Sardeshmukh, P. D., & Penland, C. (2015). Understanding the distinctively skewed and heavy tailed character of atmospheric and oceanic probability distributions. *Chaos: An Interdisciplinary Journal of Nonlinear Science*, *25*(3), 036410. https://doi.org/10.1063/1.4914169

Sardeshmukh, P. D, Penland, C, & Newman, M (2003). Drifts induced by multiplicative red noise with application to climate. *Europhysics Letters (EPL)*, *63*(4), 498–504. https://doi.org/10.1209/epl/i2003-00550-y

Sardeshmukh, P. D., & Sura, P. (2009). Reconciling non-Gaussian climate statistics with linear dynamics. *Journal of Climate*, *22*(5), 1193–1207. https://doi.org/10.1175/2008JCLI2358.1

Smith, T. M., Reynolds, R. W., Peterson, T. C., & Lawrimore, J. (2008). Improvements to NOAA's historical merged land–ocean surface temperature analysis (1880-2006). *Journal of Climate*, *21*(10), 2283–2296. https://doi.org/10.1175/2007JCLI2100.1

Su, J., Zhang, R., Li, T., Rong, X., Kug, J-S., & Hong, C.-C. (2010). Causes of the El Niño and La Niña amplitude asymmetry in the equatorial Eastern Pacific. *Journal of Climate*, *23*(3), 605–617. https://doi.org/10.1175/2009JCLI2894.1

Sura, P., & Barsugli, J. (2002). A note on estimating drift and diffusion parameters from timeseries. *Physics Letters A*, *305*(5), 304–311. https://doi.org/10.1016/S0375-9601(02)01474-3

Sura, P., & Newman, M. (2008). The impact of rapid wind variability upon air–sea thermal coupling. *Journal of Climate*, *21*(4), 621–637. https://doi.org/10.1175/2007JCLI1708.1

Sura, P., Newman, M., & Alexander, M. A. (2006). Daily to decadal sea surface temperature variability driven by state-sependent stochastic heat fluxes. *Journal of Physical Oceanography*, *36*(10), 1940–1958. https://doi.org/10.1175/JPO2948.1

Sura, P., Newman, M., Penland, C., & Sardeshmukh, P. (2005). Multiplicative noise and non-Gaussianity: A paradigm for atmospheric regimes? *Journal of the Atmospheric Sciences*, *62*(5), 1391–1409. https://doi.org/10.1175/JAS3408.1

Takahashi, K., Karamperidou, C., & Dewitte, B. (2018). A theoretical model of strong and moderate El Niño regimes. *Climate Dynamics*, *52*, 1–17. https://doi.org/10.1007/s00382-018-4100-z

Takahashi, K., Montecinos, A., Goubanova, K., & Dewitte, B. (2011). ENSO regimes: Reinterpreting the canonical and Modoki El Niño. *Geophysical Research Letters*, *38*, L10704. https://doi.org/10.1029/2011GL047364

Thomas, E. E., Vimont, D. J., Newman, M., Penland, C., & Martinez-Villalobos, C. (2018). The role of stochastic forcing in generating ENSO diversity. *Journal of Climate*, *31*, 9125–9150.

Thual, S., Majda, A. J., Chen, N., & Stechmann, S. N. (2016). Simple stochastic model for El Niño with westerly wind bursts. *Proceedings of the National Academy of Sciences of the United States of America*, *113*(37), 10,245–10,250. https://doi.org/10.1073/pnas.1612002113

Tziperman, E., Stone, L., Cane, M. A., & Jarosh, H. (1994). El Nino Chaos: Overlapping of resonances between the seasonal cycle and the Pacific ocean-atmosphere oscillator. *Science*, *264*(5155), 72–74. https://doi.org/10.1126/science.264.5155.72

Vecchi, G. A., & Harrison, D. E. (2000). Tropical Pacific sea surface temperature anomalies, El Niño, and equatorial westerly wind events*. *Journal of Climate*, *13*(11), 1814–1830. https://doi.org/10.1175/1520-0442(2000)013h1814:TPSSTAi2.0.CO;2

Vimont, D. J., Alexander, M. A., & Newman, M. (2014). Optimal growth of Central and East Pacific ENSO events. *Geophysical Research Letters*, *41*, 4027–4034. https://doi.org/10.1002/2014GL059997

Williams, P. D. (2012). Climatic impacts of stochastic fluctuations in air-sea fluxes. *Geophysical Research Letters*, *39*, L10705. https://doi.org/10.1029/2012GL051813

Wittenberg, A. T. (2009). Are historical records sufficient to constrain ENSO simulations? *Geophysical Research Letters*, *36*, L12702. https://doi.org/10.1029/2009GL038710

Xue, Y., Leetmaa, A., & Ji, M. (2000). ENSO prediction with Markov models: The impact of sea level. *Journal of Climate*, *13*(4), 849–871. https://doi.org/10.1175/1520-0442(2000)013h0849:EPWMMTi2.0.CO;2